

Multiphase Oxidation of SO₂ by NO₂ on CaCO₃ Particles

Defeng Zhao*, Xiaojuan Song*, Tong Zhu, Zefeng Zhang, Yingjun Liu

BIC-ESAT and SKL-ESPC, College of Environmental Sciences and Engineering, Peking University, Beijing, 100871, China

*These authors contributed equally to this work.

Correspondence to: Tong Zhu (tzhu@pku.edu.cn)

Abstract. Heterogeneous/multiphase oxidation of SO₂ by NO₂ on solid or aqueous particles is thought to be a potentially important source of sulfate in the atmosphere, for example, during heavily polluted episodes (haze), but the reaction mechanism and rate are uncertain. In this study, in order to assess the importance of the direct oxidation of SO₂ by NO₂ we investigated the heterogeneous/multiphase reaction of SO₂ with NO₂ on individual CaCO₃ particles in N₂ using Micro-Raman spectroscopy. In the SO₂/NO₂/H₂O/N₂ gas mixture, the CaCO₃ solid particle was first converted to the Ca(NO₃)₂ droplet by the reaction with NO₂ and the deliquescence of Ca(NO₃)₂, and then NO₂ oxidized SO₂ in the Ca(NO₃)₂ droplet forming CaSO₄, which appeared as needle-shaped crystals. Sulfate was mainly formed after the complete conversion of CaCO₃ to Ca(NO₃)₂, that is, during the multiphase oxidation of SO₂ by NO₂. The precipitation of CaSO₄ from the droplet solution promoted sulfate formation. The reactive uptake coefficient of SO₂ for sulfate formation is on the order of 10⁻⁸, and RH enhanced the uptake coefficient. We estimate that the direct multiphase oxidation of SO₂ by NO₂ is not an important source of sulfate in the ambient atmosphere compared with the SO₂ oxidation by OH in the gas phase and is not as important as other aqueous phase pathways, such as the reactions of SO₂ with H₂O₂, O₃, and O₂, with or without transition metals.

21 Sulfate is a major component of atmospheric particulate matter. It contributes to a large fraction of
22 atmospheric aerosol particles in both urban and rural areas (Seinfeld and Pandis, 2006; Zhang et al., 2007).
23 Sulfate is either from primary source, such as sea spray, or from secondary source, i.e., by the oxidation of
24 reduced sulfur compounds such as dimethyl sulfide (DMS), carbonyl sulfur (COS), and SO₂ (Seinfeld and Pandis,
25 2006). In the continent, the main source of sulfate is the oxidation of SO₂, an important air pollutant from fossil
26 fuel combustion. SO₂ can be oxidized in the gas phase, mainly by OH, or in the particle phase such as by H₂O₂,
27 O₃, or O₂ catalyzed by transition metal ions in cloud or fog water (Seinfeld and Pandis, 2006; Finlayson-Pitts and
28 Pitts Jr., 1999) or by O₃ or photochemical reactions on particle surface (Zhu et al., 2011; Li et al., 2006; Li et al.,
29 2007; Shang et al., 2010; Li et al., 2011).

30 Although various pathways of SO₂ oxidation are identified, the source of sulfate and relative importance of
31 various pathways of SO₂ oxidation forming sulfate in the atmosphere still remain uncertain. For example, during
32 heavily polluted episodes (haze) in China in recent years, high concentrations of sulfate were observed, but the
33 source of sulfate is elusive (Wang et al., 2016; Wang et al., 2014a; Zheng et al., 2015b; Guo et al., 2014). The
34 relative contribution of regional transport versus local formation and physical and chemical mechanisms
35 responsible for sulfate formation are still not clear. Recent studies have highlighted heterogeneous reactions of
36 SO₂ on solid or liquid particles to be a possibly important source of sulfate based on model, field and laboratory
37 studies (Huang et al., 2014; Zhu et al., 2011; Gao et al., 2016; Zheng et al., 2015a; Wang et al., 2014b; He et al.,
38 2014; Fu et al., 2016; Xue et al., 2016; Xie et al., 2015; Cheng et al., 2016; Wang et al., 2016). During haze
39 episodes, relative humidity (RH) is often high (Zhang et al., 2014; Wang et al., 2016; Zheng et al., 2015b) and
40 particles or some components of particles can deliquesce forming aqueous solution. In particular, several recent
41 studies propose that the multiphase oxidation of SO₂ by NO₂, another important air pollutant, on liquid particles
42 may be a major pathway of sulfate formation (Wang et al., 2016; Xue et al., 2016; Xie et al., 2015; Cheng et al.,
43 2016). Both SO₂ and NO₂ are from fossil fuel combustion and both concentrations are often high during haze
44 episodes, and their reaction may significantly contribute to sulfate formation.

45 In order to assess and quantify the role of the heterogeneous reactions of SO₂ in sulfate formation, laboratory
46 studies are needed to understand the reaction process and obtain kinetic parameters for modeling such as uptake
47 coefficients of SO₂. Among many studies investigating the heterogeneous reactions of SO₂ on various particles
48 (Goodman et al., 2001; Li et al., 2011; Shang et al., 2010; Huang et al., 2015; Huang et al., 2016; Zhou et al.,
49 2014; Li et al., 2004; Kong et al., 2014; Passananti et al., 2016; Cui et al., 2008; Chu et al., 2016; Zhao et al.,
50 2015; Li et al., 2006; Wu et al., 2011; He et al., 2014; Liu et al., 2012; Ma et al., 2008; Park and Jang, 2016;
51 Ullerstam et al., 2002; Sorimachi et al., 2001; Ullerstam et al., 2003; Wu et al., 2013; Wu et al., 2015), only a few
52 have investigated the heterogeneous reaction of SO₂ in the presence of NO₂ (He et al., 2014; Liu et al., 2012; Ma
53 et al., 2008; Park and Jang, 2016; Ullerstam et al., 2003; Ma et al., 2017). These studies found that NO₂ can
54 promote sulfate formation from SO₂ oxidation (He et al., 2014; Liu et al., 2012; Ma et al., 2008; Park and Jang,
55 2016; Ullerstam et al., 2003). However, the mechanism of this effect is still not clear and only few studies
56 reported kinetic parameters such as uptake coefficient of SO₂ due to the reaction with NO₂. Importantly, most of
57 these studies focused on the gas-solid reactions on particles. Very few laboratory studies have investigated the
58 multiphase reaction of SO₂ with NO₂ on atmospheric aqueous particles or solid-aqueous mixed phase aerosol

59 particles, and the uptake coefficient of SO₂ on atmospheric aqueous particles due to the reaction with NO₂ is
60 largely unknown. From several decades ago until now, a number of studies have investigated the aqueous
61 reaction of soluble S(IV) species (H₂SO₃, HSO₃⁻, SO₃²⁻) with NO₂ in dilute bulk solution (Lee and Schwartz,
62 1983; Clifton et al., 1988; Littlejohn et al., 1993; Takeuchi et al., 1977; Nash, 1979; Ellison and Eckert, 1984;
63 Shen and Rochelle, 1998; Tursic and Grgic, 2001) relevant to the conditions in cloud water. However, in aqueous
64 aerosol particles, the reaction rate and process may be substantially different from those in bulk solution due to
65 high ionic strength resulted from high concentrations of solutes, potential interactions of sulfate with other ions,
66 and low water activity in aerosol particles.

67 In this study, we present the finding that the multiphase reaction of SO₂ directly with NO₂ is not an
68 important source of sulfate in the atmosphere, in the absence of other oxidants such as O₂. The direct oxidation of
69 SO₂ by NO₂ pathway was proposed in a number of recent studies to be potentially important for sulfate formation
70 (Cheng et al., 2016; Wang et al., 2016; Xue et al., 2016). For example, Cheng et al. (2016) considered the direct
71 oxidation of SO₂ by NO₂ to be the most important pathway to explain the missing sulfate source during the haze
72 events in Beijing. Wang et al. (2016) also proposed that the direct oxidation of SO₂ by NO₂ is key to efficient
73 sulfate formation in the presence of high relative humidity and NH₃ and showed that in their laboratory study
74 sulfate formation is mainly contributed by the direct oxidation by NO₂ and the role of O₂ is negligible.

75 We investigated the heterogeneous reaction of SO₂ with NO₂ on CaCO₃ particles at the ambient RH. CaCO₃
76 is an important component of mineral aerosols, especially in East Asia (Cao et al., 2005; Song et al., 2005; Okada
77 et al., 2005) and it is a very reactive component (Krueger et al., 2004; Li et al., 2010; Li et al., 2006; Prince et al.,
78 2007a). It is also one of the few alkaline particles in the atmosphere, especially in northern China, which can
79 neutralize acids on particles and increase the pH of aerosol water, thus promoting the apparent solubility and
80 uptake of SO₂. The reaction of SO₂ with NO₂ on CaCO₃ has been suggested by field observations, which showed
81 internal mixing of CaCO₃, CaSO₄, and Ca(NO₃)₂ in particles (Hwang and Ro, 2006; Li and Shao, 2009; Zhang et
82 al., 2000). More importantly, as shown below, during the reaction on CaCO₃, aqueous phase can be formed,
83 which allows us to investigate the multiphase reaction of SO₂ with NO₂. We studied the reaction of SO₂ and NO₂
84 on individual CaCO₃ particles in N₂ using Micro-Raman spectrometer with a flow reaction system. N₂ was used
85 as carrier gas in order to avoid confounding effects of other oxidants including O₂ in SO₂ oxidation. Combining
86 the chemical and optical information from Micro-Raman spectrometer, we systematically investigated the
87 reaction process and quantified the reactive uptake coefficient of SO₂ due to the oxidation by NO₂ based on
88 sulfate production rate. We further assessed the importance of the multiphase oxidation of SO₂ by NO₂ in the
89 atmosphere.

90 **2 Experimental**

91 **2.1 Apparatus and procedures**

92 The experimental setup used in this study is illustrated in Fig. 1. The details of the setup have been described
93 previously (Liu et al., 2008; Zhao et al., 2011). NO₂ and SO₂ of certain concentrations were prepared by adjusting
94 the flow rates of standard gases of specified concentrations (NO₂: 1000 ppm in N₂, Messer, Germany; SO₂: 2000
95 ppm in N₂, National Institute of Metrology P.R. China) and high-purity nitrogen (99.999%, Beijing

96 Haikeyuanchang Corp.). We used N₂ as a carrier gas to exclude the potential inference from other compounds in
97 SO₂ oxidation such as O₂, which is key to investigate the direct oxidation of SO₂ by NO₂. RH was regulated by
98 adjusting the flow rates of humidified N₂ and of dry N₂ and other dry gases. Humidified N₂ was prepared by
99 bubbling N₂ through fritted glass in water. Flow rates of the gases were controlled by mass flow controllers
100 (FC-260, Tylan, Germany). Mixed gases reacted with CaCO₃ particles in a stainless steel reaction cell. Individual
101 CaCO₃ particles were deposited on a Teflon FEP film substrate annealed to a silicon wafer. The substrate was
102 then placed in the reaction cell, which has a glass cover on top of the center. Through this top window, a
103 Micro-Raman spectrometer (LabRam HR800, HORIBA Jobin Yvon) was used to acquire the Raman spectra of
104 particles. A 514 nm excitation laser was focused onto selected particles and back scattering Raman signals were
105 detected. The details of the instrument are described in previous studies (Liu et al., 2008; Zhao et al., 2011).

106 The RH and temperature of the outflow gas from the reaction cell were measured by a hygrometer (HMT100,
107 Vaisala). Experiments of individual CaCO₃ particles reacting with NO₂ (75-200 ppm) and SO₂ (75-200 ppm)
108 mixing gas diluted with N₂ were conducted under certain RH (17-72%). All the measurements were carried out at
109 25±0.5 °C. Each reaction was repeated for three times.

110 In this study, the size of CaCO₃ particles was around 7-10 μm. During a reaction, components of an
111 individual particle may distribute unevenly within the particle due to the formation of new aqueous phase or solid
112 phase, and particles may grow. Because particles are larger than the laser spot (~1.5 μm), Raman spectrum from
113 one point does not represent the chemical composition of the whole particle. Therefore Raman mapping was used
114 to obtain the spectra on different points of a particle in order to get the chemical information of the whole particle.
115 The mapping area is a rectangular slightly larger than the particle and mapping steps are 1×1 μm. Raman spectra
116 in the range 800-3900 cm⁻¹ were acquired with exposure time of 1 s for each mapping point. During each
117 mapping (7-10 min, depending on the mapping area), no noticeable change in composition was detected. The
118 mean time of a mapping period was used as reaction time. During the reaction, microscopic images of particles
119 were also recorded. Raman spectra were analyzed using Labspec 5 software (HORIBA Jobin Yvon). Raman
120 peaks were fit to Gaussian-Lorentzian functions to obtain peak positions and peak areas on different points of the
121 particle. The peak areas were then added up to get the peak area for the whole particle.

122 Besides the reaction of CaCO₃ with SO₂ and NO₂, other reaction systems including the reaction on Ca(NO₃)₂,
123 NaNO₃, and NH₄NO₃ particles with SO₂ or SO₂ and NO₂ mixing gas (summarized in Table 1) were also studied
124 in order to elucidate the reaction mechanism. Most experiments were conducted using CaCO₃ particles rather
125 than directly using Ca(NO₃)₂ particles. CaCO₃ was selected because it is an important component of mineral
126 aerosols especially in China as mentioned in the introduction and often used as a surrogate of mineral aerosols.
127 Moreover, using CaCO₃ particles can better simulate the reaction on internally-mixed
128 CaCO₃(solid)-Ca(NO₃)₂(aqueous) particles, which is widely observed in the ambient atmosphere and laboratory
129 (Laskin et al., 2005; Zhang et al., 2003; Li and Shao, 2009; Sullivan et al., 2007; Li et al., 2010; Liu et al., 2008),
130 and is formed via the reaction of CaCO₃ with acidic gases such as HNO₃ and NO₂ due to its alkalinity.

131 CaCO₃ (98%, Sigma) with diameters about 7-10 μm on average, Ca(NO₃)₂·4H₂O (ACS, 99-103%; Riedel-de
132 Haën), NH₄NO₃ (AR, Beijing Chemical Works), and NaNO₃ (AR, Beijing Chemical Works) were used without
133 further purification.

134 2.2 Quantification of reaction products on the particle phase

135 The Raman intensity of a sample is described as Equation (1):

$$136 I(\nu)=I_0 \cdot A(\nu) \cdot J(\nu) \cdot \nu^4 \cdot D \cdot K \quad (1)$$

137 where I_0 is the intensity of incident laser, $A(\nu)$ is the collection efficiency function of a Raman spectrometer,
138 $J(\nu) \cdot \nu^4$ is the Raman scattering section of the sample, D is the number density of the sample, and K is the
139 effective depth of the sample. Raman intensity is not only determined by the amount of the sample molecules, but
140 also by the configuration of the instrument, whose influence cannot be eliminated unless internal standards are
141 used. For soluble compounds, water can be used an internal standard (Zhao et al., 2011; Liu et al., 2008).
142 However, in this study, one product (CaSO_4 , see below) appeared as solid state. For solid particles of micro-scale,
143 it is hard to add internal standards into the system. Therefore it is difficult to establish the relationship between
144 Raman intensity and the amount of sample molecules, which makes the quantification very challenging.

145 In this study, we chose seven individual CaSO_4 particles varying in size as the standard for solid products.
146 The profile of each particle can be obtained by scanning the particle using Raman mapping with steps of 1, 1, and
147 2 μm for x, y, and z dimension, respectively. The volume of each particle was calculated based on 3D profiles of
148 the particles using a CAD software (AutoDesk). In order to minimize the influence of variations of incident laser
149 on Raman intensity, these seven particles were measured before each experiment, which produced a calibration
150 curve for each experiment (Fig. S1).

151 2.3 Determination of reactive uptake coefficient

152 In this study, sulfate was produced from the oxidation of SO_2 . The reactive uptake coefficient γ of SO_2 on
153 individual particles was estimated from sulfate formation. γ is derived as the rate of sulfate formation
154 ($d\{\text{SO}_4^{2-}\}/dt$) divided by the rate of surface collisions with an individual particle (Z),

$$155 \gamma = \frac{d\{\text{SO}_4^{2-}\}}{dt} \cdot \frac{1}{Z} \quad (2)$$

$$156 Z = \frac{1}{4} c A_s [\text{SO}_2], \quad (3)$$

$$157 c = \sqrt{\frac{8RT}{\pi M_{\text{SO}_2}}}, \quad (4)$$

158 where R is the gas constant, T is temperature, M_{SO_2} is the molecular weight of SO_2 , and c is the mean
159 molecular velocity of SO_2 , A_s is the surface area of an individual particle. Z is the collision rate between SO_2 and
160 a particle. $\{\text{SO}_4^{2-}\}$ indicates the amount of sulfate on the particle phase in mole, and $[\text{SO}_2]$ indicates the
161 concentration of SO_2 in the gas phase.

162 $\{\text{SO}_4^{2-}\}$ was determined by a calibration curve as stated above. In this study, since sulfate was mainly
163 formed after the formation of $\text{Ca}(\text{NO}_3)_2$ droplet as shown below, A_s was calculated by estimating the diameter of
164 the droplet according to its microscopic image and using a shape of spherical segment defined by the contact
165 angle of a water droplet on Teflon (Good and Koo, 1979). For each experiment, at least three particles with
166 different diameters were measured to get an average reactive uptake coefficient.

168 **3.1 Reaction products and particle morphology changes**

169 Figure 2 shows typical Raman spectra of a CaCO_3 particle during the reaction with SO_2 and NO_2 . The peak
170 at 1087 cm^{-1} is assigned to the symmetric stretching mode of carbonate (ν_1) (Nakamoto, 1997), which could be
171 detected during the initial stage of the reaction. Shortly after the reaction started, a peak at 1050 cm^{-1} was
172 observed, which is attributed to the symmetric stretching mode of nitrate (ν_1). This demonstrates that calcium
173 nitrate ($\text{Ca}(\text{NO}_3)_2$) was produced during the reaction. A broad band at $2800\text{--}3800\text{ cm}^{-1}$ was also observed together
174 with the formation of $\text{Ca}(\text{NO}_3)_2$. It is assigned to $-\text{OH}$ stretching of water in aqueous solution. The formation of
175 aqueous solution is attributed to the deliquescence of $\text{Ca}(\text{NO}_3)_2$, which is very hygroscopic and can deliquesce at
176 $\sim 10\%$ RH (Liu et al., 2008; Al-Abadleh et al., 2003; Tang and Fung, 1997). After about 82 min, a new peak at
177 1013 cm^{-1} was observed, which is attributed to the symmetric stretching mode of sulfate (ν_1) in anhydrite (CaSO_4)
178 (Sarma et al., 1998). This peak clearly demonstrates that sulfate was formed. CaSO_4 as a reaction product has
179 also been found in the reaction of CaCO_3 with SO_2 and NO_2 in a previous study (Ma et al., 2013b). Afterwards,
180 no other Raman peaks than those of CaCO_3 , $\text{Ca}(\text{NO}_3)_2$, and CaSO_4 were detected until 1050 min after the
181 reaction.

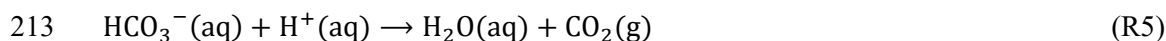
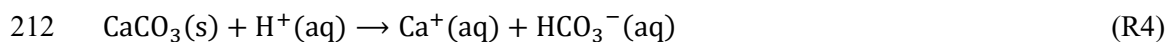
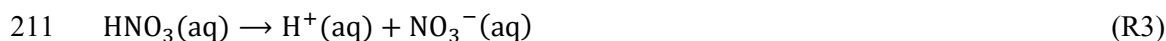
182 Concomitant with the formation of $\text{Ca}(\text{NO}_3)_2$ and CaSO_4 , the microscopic morphology of the particle
183 changed significantly. The initial CaCO_3 particle was a crystal close to a rhombohedron of about $9\text{--}10\text{ }\mu\text{m}$ (Fig.
184 3a). After reacting with NO_2/SO_2 , the surface of the particle became smoother, and then a liquid layer formed
185 surrounding the solid particle core (Fig. 3c). Raman spectra of the particle reveal that the outer liquid layer
186 consisted of $\text{Ca}(\text{NO}_3)_2$ and water. As the reaction proceeded, the solid CaCO_3 core diminished gradually and
187 finally CaCO_3 completely disappeared and a $\text{Ca}(\text{NO}_3)_2$ spherical droplet was formed (Fig. 3d). The whole particle
188 became larger due to the growth of the outer liquid layer. The diameter of the $\text{Ca}(\text{NO}_3)_2$ droplet reached $\sim 16\text{ }\mu\text{m}$,
189 and the droplet did not change much in the subsequent period of the reaction. Despite the invariant droplet
190 diameter, a new solid phase of needle-shaped crystals was formed as the reaction proceeded, which distributed
191 unevenly in the droplet. The Raman spectra of the new solid phase and Raman mapping (Fig. S2) reveal that this
192 solid matter was CaSO_4 . The amount of CaSO_4 increased gradually during the reaction, and its Raman peak could
193 be observed more clearly at 1050 min.

194 **3.2 Reaction process**

195 In order to learn about the reaction process and mechanism, the amounts of $\text{Ca}(\text{NO}_3)_2$, CaSO_4 , and CaCO_3 ,
196 represented by the peak area at 1050 , 1013 , and 1087 cm^{-1} in Raman spectra, respectively, were investigated as a
197 function of reaction time. As shown in Fig. 4, $\text{Ca}(\text{NO}_3)_2$ was produced before CaSO_4 . Nitrate was detected
198 immediately after the reaction started, and reached a maximum at ~ 50 min whereas sulfate did not reach the
199 detection limit until 82 min of the reaction. Sulfate increased slowly in the reaction and we did not observe it
200 leveling off even after 1050 min.

201 According to the time series of carbonate, nitrate, and sulfate, this reaction consisted of two successive
202 processes. The first process was the formation of $\text{Ca}(\text{NO}_3)_2$, which was accompanied with the decline of CaCO_3
203 (Fig. 4), indicating that $\text{Ca}(\text{NO}_3)_2$ was produced due to the reaction of CaCO_3 with NO_2 . $\text{Ca}(\text{NO}_3)_2$ has been

204 observed in the reaction of CaCO₃ with NO₂ in previous studies (Li et al., 2010; Tan et al., 2017). The formation
205 of Ca(NO₃)₂ started with the reaction of NO₂ with adsorbed water or water in aqueous solution, forming HNO₃
206 and HNO₂. Then HNO₃ reacted with CaCO₃ forming Ca(NO₃)₂ as well as CO₂, which was released to the gas
207 phase. HNO₂ could evaporate into the gas phase due to the continuous flushing of reactant gases during the
208 experiments and acidity of the droplet (see below). The reaction equations are as follows:



215 The detailed mechanism of the formation of Ca(NO₃)₂ in the reaction CaCO₃ with NO₂ have been studied by Li et
216 al. (2010).

217 The second process was the formation of CaSO₄ through the oxidation of SO₂ by NO₂. CaSO₄ was mainly
218 produced after CaCO₃ was completely reacted and increased steadily as the reaction proceeded. The amount of
219 Ca(NO₃)₂ as the product of NO₂ uptake was overwhelmingly higher than that of CaSO₄ as the product of the
220 reaction SO₂ with NO₂, which only reached detection limit after the complete conversion of CaCO₃. This
221 indicates that the reaction of SO₂ with NO₂ did not contribute significantly to NO₂ uptake before CaCO₃
222 completely converted to Ca(NO₃)₂. Afterwards, the reaction of SO₂ with NO₂ promoted the reactive uptake of
223 NO₂ by Ca(NO₃)₂ droplet.

224 3.3 Reaction mechanism

225 3.3.1 Mechanism of sulfate formation

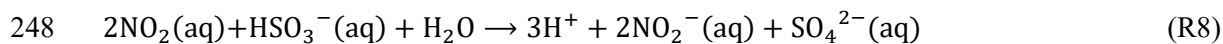
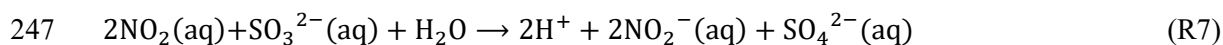
226 Based on the results above, we found that a series of reactions of SO₂ and NO₂ on a CaCO₃ particle led to
227 sulfate formation. Almost the entire sulfate was produced after a CaCO₃ particle was converted to a Ca(NO₃)₂
228 droplet (Fig. 4), although in some experiments a trace amount of sulfate could be observed when a small amount
229 of CaCO₃ was still left in the Ca(NO₃)₂ droplet. The absence or low amount of sulfate before CaCO₃ was
230 completely reacted might be due to the competition between the reaction of aqueous NO₂ with CaCO₃ and the
231 reaction with SO₂. This result suggests that forming a Ca(NO₃)₂ droplet was key to the formation of sulfate.

232 This finding is further supported by the results of the reaction of SO₂ with NO₂ on a Ca(NO₃)₂ droplet (Fig. 5
233 and Table 1). Using a Ca(NO₃)₂ droplet as the reactant, the reaction with SO₂/NO₂ at the same condition still
234 produced CaSO₄, confirming CaCO₃ was not necessary for sulfate formation. The reaction with Ca(NO₃)₂
235 produced similar amount of sulfate to the reaction with CaCO₃ based on Raman spectra and microscopic images
236 (Fig. 5), which indicates that Ca(NO₃)₂ droplet was important for sulfate formation. Therefore, we conclude that
237 SO₂ was mainly oxidized via the multiphase reaction on the Ca(NO₃)₂ droplet while CaCO₃ mainly worked as a
238 precursor of the Ca(NO₃)₂ droplet.

239 The oxidant of SO₂ can be NO₃⁻ or NO₂ in the Ca(NO₃)₂ droplet here. In a reaction between Ca(NO₃)₂
240 droplets and SO₂ (150 ppm) under 72% RH, we did not observe any sulfate formation on the basis of the Raman

241 spectra and microscopic image after 5 h of reaction. This indicates that NO_3^- was not the oxidant for SO_2 in our
242 study, which was also consistent with a previous study (Martin et al., 1981). Therefore, we conclude that SO_2 was
243 oxidized by NO_2 in the $\text{Ca}(\text{NO}_3)_2$ droplet.

244 According to previous studies, NO_2 can oxidize sulfite and bisulfite ions into sulfate ion in aqueous phase
245 (Ellison and Eckert, 1984; Shen and Rochelle, 1998; Littlejohn et al., 1993). The overall reaction equation was
246 described to be (Clifton et al., 1988):



249 Under the experimental conditions of our study, water uptake of $\text{Ca}(\text{NO}_3)_2$ led to condensation of water, which
250 provided a site for aqueous oxidation of S(IV) by NO_2 . The relative fractions of the three S(IV) species depend
251 on pH and the equilibrium between them is fast (Seinfeld and Pandis, 2006). The pH of the droplet was mainly
252 determined by the gas-aqueous equilibrium of SO_2 in this study and estimated to be ~ 3 . The characteristic time to
253 reach the equilibrium in the gas-particle interface ($\sim 10^{-5}$ s) was estimated to be much less than the characteristic
254 time for the aqueous phase reaction of SO_2 with NO_2 (10^{-2} - 10^{-1} s) (Supplement S2). Therefore, aqueous S(IV)
255 species can be considered to be in equilibrium with SO_2 in the gas phase. The concentrations of HSO_3^- , H_2SO_3 ,
256 and SO_3^{2-} were estimate to be $\sim 1.1 \times 10^{-3}$, 9.2×10^{-5} , and 6.6×10^{-8} mol L^{-1} , respectively, using the equilibrium
257 constants in Seinfeld and Pandis (2006) ($H_{\text{SO}_2} = 1.23$ mol L^{-1} atm $^{-1}$, $K_1 = 1.3 \times 10^{-2}$ mol L^{-1} , $K_2 = 6.6 \times 10^{-8}$ mol L^{-1}) and
258 thus the main S(IV) species was HSO_3^- . Then SO_4^{2-} from S(IV) oxidation can react with Ca^{2+} forming CaSO_4
259 precipitation as observed in Raman spectra due to the low value of K_{sp} for CaSO_4 (Lide, 2009):



261 Some previous studies have shown that SO_2 can react with CaCO_3 to produce calcium sulfite (CaSO_3) (Li et
262 al., 2006; Prince et al., 2007b; Ma et al., 2013a), and CaSO_3 can be oxidized to CaSO_4 by NO_2 (Rosenberg and
263 Grotta, 1980; Ma et al., 2013a). In our study, we investigated the reaction between CaCO_3 and SO_2 (150 ppm) at
264 72% RH. We found that both sulfate and sulfite were lower than the detection limit of our Raman spectrometer
265 ($\sim 5 \times 10^{-14}$ mol for sulfate at a signal to noise ratio of 2 and $\sim 3 \times 10^{-14}$ mol for sulfite according to the relative
266 Raman scattering cross-section of sulfate and sulfite (Meyer et al., 1980)) even after 300 min of the reaction. This
267 indicates that forming CaSO_3 was not the main pathway in CaSO_4 formation in our study and CaCO_3 did not
268 directly contribute to the formation of CaSO_4 .

269 3.3.2 Effects of cations in sulfate formation

270 Since sulfate was observed to precipitate as CaSO_4 , we further analyzed the effect of precipitation reaction
271 and cations on the aqueous oxidation of SO_2 by NO_2 . In order to test effects of cations, we replaced Ca^{2+} with Na^+
272 or NH_4^+ . Based on Raman spectra, we found that in the reaction of a NaNO_3 or a NH_4NO_3 droplet with NO_2/SO_2 ,
273 sulfate, either as aqueous ion (at 984 cm^{-1} and 979 cm^{-1} for $(\text{NH}_4)_2\text{SO}_4$ and Na_2SO_4 , respectively) or as in CaSO_4
274 crystal, was below the detection limit after 300 min in the same reaction conditions as $\text{Ca}(\text{NO}_3)_2$ and CaCO_3 (Fig.
275 6 and Table 1). Considering that the Raman scattering cross-section of sulfate in $(\text{NH}_4)_2\text{SO}_4$ aqueous aerosol
276 particle is even higher than sulfate in CaSO_4 (Wright, 1973; Stafford et al., 1976), it can be concluded that the
277 sulfate production rate was larger in the presence of Ca^{2+} compared to those in the presence of Na^+ or NH_4^+ . The

278 difference can be explained by two possible reasons. The first possible reason may be due to the change of Gibbs
 279 energy. The spontaneity of the SO₂ oxidation by NO₂ for Reaction (R8) can be analyzed using the reaction Gibbs
 280 energy as follows:

$$281 \quad \Delta_r G = \Delta_r G^\theta + RT \ln \frac{a_{H^+}^3 \cdot a_{SO_4^{2-}} \cdot a_{NO_2^-}^2}{a_{NO_2(aq)}^2 \cdot a_{HSO_3^-}} \quad (5)$$

282 where $\Delta_r G$ is the reaction Gibbs energy, $\Delta_r G^\theta$ is the standard reaction Gibbs energy, R is the gas constant, T
 283 is temperature, and a is the activity of various species.

284 $\Delta_r G$ increases with increasing sulfate concentration. According to the different results between the reaction
 285 on Ca(NO₃)₂ droplet and the reaction on NaNO₃ and NH₄NO₃ droplet, there might be a backward reaction of SO₂
 286 oxidation which consumed sulfate, although the detailed mechanism of the backward reaction is unknown at the
 287 moment. For NaNO₃ and NH₄NO₃ droplet, once sulfate concentration reached certain level, the reaction may stop
 288 due to the increase of $\Delta_r G$. For Ca(NO₃)₂ droplet, the precipitation of CaSO₄ can substantially decrease the
 289 activity of SO₄²⁻, and thus decrease $\Delta_r G$ and promote the oxidation of SO₂ and sulfate formation. The second
 290 possible reason is that sulfate may crowd the reaction environment and suppress the colliding probability of S(IV)
 291 species with NO₂ in aqueous phase and the uptake coefficient of SO₂ or NO₂ on the droplet. Precipitation of
 292 sulfate as CaSO₄ can cancel such suppressions and thus promote the reaction. Regardless of the reasons behind,
 293 we can conclude that the precipitation of less soluble CaSO₄ promoted sulfate formation.

294 3.4 Reactive uptake coefficient of SO₂

295 The reactive uptake coefficients of SO₂ (γ) for sulfate formation under different conditions are shown in
 296 Table 2. Each reaction was repeated for three times, during which, three particles with different size were
 297 selected. γ was higher at higher relative humidity, suggesting again that water in aqueous solution plays an
 298 important role in the formation of CaSO₄. At 17% RH, the reaction between CaCO₃ and NO₂ (the first process of
 299 the whole reaction) proceeded very slowly, and the amount of water in aqueous solution formed due to the water
 300 uptake of Ca(NO₃)₂ was very low. As a result, we did not observe the formation of CaSO₄ (the second process of
 301 the whole reaction) after 1000 min of the reaction and even at higher SO₂ and NO₂ concentrations (200 ppm SO₂,
 302 200 ppm NO₂). Under higher relative humidity (46% and 72% RH), sulfate was observed soon after the reaction.
 303 It is interesting to note that there were no significant difference for γ between 46% and 72% RH. In either case,
 304 the reaction between CaCO₃ and NO₂ proceeded quickly and CaCO₃ was completely converted to a Ca(NO₃)₂
 305 droplet within 100 min after the reaction. In the presence of enough water in aqueous solution, RH seemed to be
 306 no longer a limiting factor. In such conditions, an increase of NO₂ concentration (from 75 ppm to 200 ppm at 72%
 307 RH) promoted the reactive uptake of SO₂.

308 The reactive uptake coefficient of SO₂ for sulfate formation was determined to be on the order of 10⁻⁸ at 46%
 309 and 72% RH. This value is higher than the uptake coefficient (10⁻¹⁰) on mineral particles sampled from Cape
 310 Verde Islands (the main contents being potassium feldspars and quartz) obtained by Ullerstam et al. (2003) using
 311 NO₂/SO₂ mixing gas and Diffuse Reflectance Infrared Fourier Transform Spectroscopy (DRIFTS) technique. But
 312 the uptake coefficient in this study is lower than the uptake coefficient of SO₂ on Arizona Test Dust (ATD)
 313 particles in the presence of NO₂ ((2.10±0.08)×10⁻⁶) determined by Park and Jang (2016). γ here is also much
 314 lower than the γ of SO₂ on oxalic acid particles in the presence of NO₂ and NH₃ (10⁻⁶~10⁻⁴) determined at varying

315 RH reported by Wang et al. (2016). The difference in these uptake coefficients is attributed to the different
316 chemical composition of particles, reaction mechanism, reaction conditions, and the ways that the particle surface
317 is determined. It is worth noting that in the studies of Ullerstam et al. (2003) and Park and Jang (2016), particles
318 exist as solid state and sulfate formation is via gas-solid heterogeneous reaction, and in the study of Wang et al.
319 (2016) sulfate formation is stated to be via aqueous reaction. In this study sulfate formation was via
320 gas-liquid-solid multiphase reaction and water in aqueous solution played a key role.

321 The γ of SO_2 was further compared with the reaction rate constants of the aqueous reaction of NO_2 with
322 sulfite and bisulfite in bulk solution in the literature by deriving γ from rate constants using the method in
323 Davidovits et al. (2006). The detailed method can be referred to the supplement S1. Lee and Schwartz (1983)
324 determined the rate constant of the reaction of NO_2 with bisulfite to be $>2 \times 10^6 \text{ mol}^{-1} \text{ L s}^{-1}$ at pH 5.8 and 6.4.
325 Clifton et al. (1988) determined the rate constant of the reaction of NO_2 with sulfite/bisulfite to be
326 $(1.24\text{-}2.95) \times 10^7 \text{ mol}^{-1} \text{ L s}^{-1}$ at pH 5.6-13 and further reported a rate constant of $1.4 \times 10^5 \text{ mol}^{-1} \text{ L s}^{-1}$ at pH 5 from
327 the study of Lee and Schwartz (1983). The different rate constants were attributed to the different approaches to
328 determine the reaction rate by Clifton et al. (1988). Clifton et al. (1988) determined the reaction rate from the
329 consumption rate the reactant, NO_2 , which corresponds to the first reaction step of NO_2 with S(IV). Yet, Lee and
330 Schwartz (1983) determined the reaction rate from the production rate of products (their conductivity), which is
331 expected to be much slower than NO_2 consumption since formation of products needs more steps. In this study,
332 we determined γ using sulfate production rate, and thus our data are comparable to the study of Lee and Schwartz
333 (1983). Yet, the study of Lee and Schwartz (1983) only covers a pH range of 5-6.4 and has no overlap with the
334 pH (~ 3) in our study, therefore uptake coefficients from both studies are not directly comparable. Nevertheless,
335 the reaction rate of $1.4 \times 10^5 \text{ mol}^{-1} \text{ L s}^{-1}$ at pH 5 corresponds to the uptake coefficient of 4.3×10^{-7} , which is around
336 one order of magnitude higher than the uptake coefficient in our study determined at pH ~ 3 for the droplet. The
337 difference may be due to the different pH between these two studies, the different mechanisms between the
338 multiphase reaction on particles and bulk aqueous reaction, and the different concentrations of each S(IV) species
339 since the different species may have different reactivity with NO_2 . The reaction rate of S(IV) has been found to
340 decrease with decreasing pH and the reactivity of sulfite with NO_2 seems to be higher than bisulfite (Lee and
341 Schwartz, 1983; Clifton et al., 1988; Takeuchi et al., 1977). In addition, the ionic strength in the droplet of this
342 study ($15\text{-}55 \text{ mol Kg}^{-1}$) was much higher than that in the bulk solution in previous studies (on the order of
343 $10^{-6}\text{-}10^{-1} \text{ mol Kg}^{-1}$), which may also influence the reaction rate.

344 In the ambient atmosphere, the reactive uptake coefficient of SO_2 due to the multiphase oxidation by NO_2 is
345 influenced by various factors such as RH, NO_2 concentration, pH, sulfate concentration, and the presence of other
346 ions in aerosol particles. For example, NO_2 concentrations in the atmosphere are much lower than those used in
347 this study. At lower NO_2 concentrations, the uptake coefficient of SO_2 decreases, because the oxidation rate of
348 SO_2 in aqueous phase decreases with decreasing NO_2 concentration. In addition, aqueous sulfate concentrations
349 in aerosol particles in the atmosphere are often high. According to the effect of cations (Section 3.3.2), while
350 reduced sulfate concentration by CaSO_4 precipitation likely led to the enhanced sulfate production rate in the
351 reaction of SO_2 on $\text{Ca}(\text{NO}_3)_2$, higher sulfate concentration could increase the reaction Gibbs energy $\Delta_r G$ (as
352 shown in Eq. 5) and reduce the colliding probability of S(IV) species with NO_2 in the aqueous phase as discussed
353 above and thus suppress the reaction of SO_2 and NO_2 . This can reduce the uptake coefficient of SO_2 . Therefore,

354 the reactive uptake coefficient of SO₂ obtained in this study (10⁻⁸ at 46-72% RH and 75 ppm NO₂) can be
355 regarded as an upper limit of the reactive uptake coefficient of SO₂ due to the multiphase reaction with NO₂ in
356 the ambient atmosphere.

357 4 Conclusion and implications

358 We investigated the heterogeneous reaction of SO₂ directly with NO₂ on individual CaCO₃ particles in N₂
359 using Micro-Raman spectrometry. The reaction first converted the CaCO₃ particle to the Ca(NO₃)₂ droplet via the
360 reaction with NO₂ in the SO₂/NO₂/H₂O/N₂ gas mixture and the deliquescence of Ca(NO₃)₂, and then formed
361 needle-shaped CaSO₄ crystals in the Ca(NO₃)₂ droplet via the multiphase reaction of SO₂ with NO₂. The sulfate
362 formation was observed only during the multiphase oxidation by NO₂, that is, after the complete conversion of
363 CaCO₃ to Ca(NO₃)₂ droplet. The precipitation of CaSO₄ from solution promoted sulfate formation. The reactive
364 uptake coefficient of SO₂ for sulfate formation in the multiphase reaction with NO₂ is on the order of 10⁻⁸ under
365 the experimental conditions of this study (RH: 46-72%, NO₂: 75 ppm). The reactive uptake coefficient of SO₂
366 was found to be enhanced at higher RH.

367 In order to assess the importance of the multiphase reaction of SO₂ directly oxidized by NO₂ to sulfate in the
368 atmosphere, we compare the lifetime of SO₂ due to the multiphase oxidation of SO₂ by NO₂ with the lifetime due
369 to the gas phase oxidation of SO₂ by OH. Using a daytime OH concentration of 1×10⁶ molecule cm⁻³ (Lelieveld
370 et al., 2016; Prinn et al., 2005), the lifetime of SO₂ in the atmosphere due to gas phase OH oxidation is around 12
371 days. The life time of SO₂ due to the multiphase oxidation by NO₂ is around 7000 days using the uptake
372 coefficient of SO₂ from this study (3.22×10⁻⁸) and a typical particle surface area concentration for mineral
373 aerosols in winter in Beijing (6.3×10⁻⁶ cm² cm⁻³) (Huang et al., 2015). Using an annual average particle surface
374 area concentration of PM₁₀ in Beijing (1.4×10⁻⁵ cm² cm⁻³) (Wehner et al., 2008) results in a SO₂ life time of 3300
375 days due to the multiphase oxidation by NO₂. In the atmosphere, the lifetime of SO₂ due to the multiphase
376 oxidation by NO₂ should be even longer than these values because the uptake coefficient of SO₂ used here
377 (3.22×10⁻⁸) is an upper limit of the uptake coefficient of SO₂ in the ambient atmosphere as discussed above. This
378 comparison indicates that the direct multiphase oxidation of SO₂ by NO₂ is unlikely to be an important sink of
379 SO₂ and source of sulfate compared with the oxidation of SO₂ by OH.

380 It is worth mentioning that this study did not investigate the dependence of the reactive uptake coefficient
381 due to the direct oxidation of SO₂ by NO₂ on pH, especially not under high pH conditions, for which recent
382 studies have claimed this reaction to be important (Cheng et al., 2016; Wang et al., 2016). Because of the
383 important role of multiphase/heterogeneous reactions in SO₂ oxidation found in the atmosphere and the low
384 reaction rate of the direct multiphase oxidation of SO₂ by NO₂, it is more likely that the aqueous reactions of SO₂
385 with other oxidants, such as the reactions with H₂O₂, O₃, and O₂, with or without transition metals, could be
386 important pathways for sulfate formation in the atmosphere.

387 Acknowledgements

388 This work was supported by Natural Science Foundation Committee of China (41421064, 21190051, and
389 40490265) and Ministry of Science and Technology (Grant No. 2002CB410802).

390 **References**

- 391 Al-Abadleh, H. A., Krueger, B. J., Ross, J. L., and Grassian, V. H.: Phase transitions in calcium nitrate thin films,
392 Chem. Commun. , 2796-2797, 2003.
- 393 Bougiatioti, A., Nikolaou, P., Stavroulas, I., Kouvarakis, G., Weber, R., Nenes, A., Kanakidou, M., and
394 Mihalopoulos, N.: Particle water and pH in the eastern Mediterranean: source variability and implications for
395 nutrient availability, Atmos. Chem. Phys., 16, 4579-4591, 10.5194/acp-16-4579-2016, 2016.
- 396 Cao, J. J., Lee, S. C., Zhang, X. Y., Chow, J. C., An, Z. S., Ho, K. F., Watson, J. G., Fung, K., Wang, Y. Q., and
397 Shen, Z. X.: Characterization of airborne carbonate over a site near Asian dust source regions during spring 2002
398 and its climatic and environmental significance, J. Geophys. Res.-Atmos. , 110, 10.1029/2004jd005244, 2005.
- 399 Cheng, Y. F., Zheng, G. J., Wei, C., Mu, Q., Zheng, B., Wang, Z. B., Gao, M., Zhang, Q., He, K. B., Carmichael,
400 G., Poschl, U., and Su, H.: Reactive nitrogen chemistry in aerosol water as a source of sulfate during haze events
401 in China, Sci. Adv., 2, 10.1126/sciadv.1601530, 2016.
- 402 Chu, B. W., Zhang, X., Liu, Y. C., He, H., Sun, Y., Jiang, J. K., Li, J. H., and Hao, J. M.: Synergetic formation of
403 secondary inorganic and organic aerosol: effect of SO₂ and NH₃ on particle formation and growth, Atmos. Chem.
404 Phys., 16, 14219-14230, 10.5194/acp-16-14219-2016, 2016.
- 405 Clifton, C. L., Altstein, N., and Huie, R. E.: Rate-constant for the reaction of NO₂ with sulfur(IV) over the pH
406 range 5.3-13, Environ. Sci. Technol., 22, 586-589, 10.1021/es00170a018, 1988.
- 407 Cui, H. X., Cheng, T. T., Chen, J. M., Xu, Y. F., and Fang, W.: A Simulated Heterogeneous Reaction of SO₂ on
408 the Surface of Hematite at Different Temperatures, Acta Phys. Chim. Sin. , 24, 2331-2336,
409 10.3866/pku.whxb20081231, 2008.
- 410 Davidovits, P., Kolb, C. E., Williams, L. R., Jayne, J. T., and Worsnop, D. R.: Mass accommodation and
411 chemical reactions at gas-liquid interfaces, Chem. Rev., 106, 1323-1354, 10.1021/cr040366k, 2006.
- 412 Ellison, T. K., and Eckert, C. A.: The oxidation of aqueous sulfur dioxide. 4. The influence of nitrogen dioxide at
413 low pH, J. Phys. Chem., 88, 2335-2339, 10.1021/j150655a030, 1984.
- 414 Finlayson-Pitts, B., and Pitts Jr., J.: Chemistry of the upper and lower atmosphere: theory, experiments, and
415 applications, Academic Press San Diego, 969 pp., 1999.
- 416 Fu, X., Wang, S. X., Chang, X., Cai, S. Y., Xing, J., and Hao, J. M.: Modeling analysis of secondary inorganic
417 aerosols over China: pollution characteristics, and meteorological and dust impacts, Sci. Rep., 6,
418 10.1038/srep35992, 2016.
- 419 Gao, M., Carmichael, G. R., Wang, Y., Ji, D., Liu, Z., and Wang, Z.: Improving simulations of sulfate aerosols
420 during winter haze over Northern China: the impacts of heterogeneous oxidation by NO₂, Front. Environ. Sci.
421 Eng., 10, 16, 10.1007/s11783-016-0878-2, 2016.
- 422 Good, R. J., and Koo, M. N.: Effect of drop size on contact-angle, J. Colloid Interface Sci. , 71, 283-292, 1979.
- 423 Goodman, A. L., Li, P., Usher, C. R., and Grassian, V. H.: Heterogeneous uptake of sulfur dioxide on aluminum
424 and magnesium oxide particles, J. Phys. Chem. A 105, 6109-6120, 2001.
- 425 Guo, H., Sullivan, A. P., Campuzano-Jost, P., Schroder, J. C., Lopez-Hilfiker, F. D., Dibb, J. E., Jimenez, J. L.,
426 Thornton, J. A., Brown, S. S., Nenes, A., and Weber, R. J.: Fine particle pH and the partitioning of nitric acid
427 during winter in the northeastern United States, J. Geophys. Res.-Atmos. , 121, 10355-10376,
428 10.1002/2016jd025311, 2016.

429 Guo, H., Weber, R. J., and Nenes, A.: High levels of ammonia do not raise fine particle pH sufficiently to yield
430 nitrogen oxide-dominated sulfate production, *Sci. Rep.*, 7, 12109, 10.1038/s41598-017-11704-0, 2017a.

431 Guo, H. Y., Liu, J. M., Froyd, K. D., Roberts, J. M., Veres, P. R., Hayes, P. L., Jimenez, J. L., Nenes, A., and
432 Weber, R. J.: Fine particle pH and gas-particle phase partitioning of inorganic species in Pasadena, California,
433 during the 2010 CalNex campaign, *Atmos. Chem. Phys.*, 17, 5703-5719, 10.5194/acp-17-5703-2017, 2017b.

434 Guo, S., Hu, M., Zamora, M. L., Peng, J., Shang, D., Zheng, J., Du, Z., Wu, Z., Shao, M., Zeng, L., Molina, M. J.,
435 and Zhang, R.: Elucidating severe urban haze formation in China, *Proc. Nat. Acad. Sci. U.S.A.*, 111,
436 17373-17378, 10.1073/pnas.1419604111, 2014.

437 He, H., Wang, Y., Ma, Q., Ma, J., Chu, B., Ji, D., Tang, G., Liu, C., Zhang, H., and Hao, J.: Mineral dust and
438 NO_x promote the conversion of SO₂ to sulfate in heavy pollution days, *Sci. Rep.*, 4, 10.1038/srep04172, 2014.

439 Huang, L., Zhao, Y., Li, H., and Chen, Z.: Kinetics of Heterogeneous Reaction of Sulfur Dioxide on Authentic
440 Mineral Dust: Effects of Relative Humidity and Hydrogen Peroxide, *Environ. Sci. Technol.*, 49, 10797-10805,
441 10.1021/acs.est.5b03930, 2015.

442 Huang, L. B., Zhao, Y., Li, H., and Chen, Z. M.: Hydrogen peroxide maintains the heterogeneous reaction of
443 sulfur dioxide on mineral dust proxy particles, *Atmos. Environ.*, 141, 552-559, 10.1016/j.atmosenv.2016.07.035,
444 2016.

445 Huang, X., Song, Y., Zhao, C., Li, M., Zhu, T., Zhang, Q., and Zhang, X.: Pathways of sulfate enhancement by
446 natural and anthropogenic mineral aerosols in China, *J. Geophys. Res.-Atmos.*, 119, 14,165-114,179,
447 10.1002/2014jd022301, 2014.

448 Hwang, H. J., and Ro, C. U.: Direct observation of nitrate and sulfate formations from mineral dust and sea-salts
449 using low-Z particle electron probe X-ray microanalysis, *Atmos. Environ.*, 40, 3869-3880,
450 10.1016/j.atmosenv.2006.02.022, 2006.

451 Kong, L. D., Zhao, X., Sun, Z. Y., Yang, Y. W., Fu, H. B., Zhang, S. C., Cheng, T. T., Yang, X., Wang, L., and
452 Chen, J. M.: The effects of nitrate on the heterogeneous uptake of sulfur dioxide on hematite, *Atmos. Chem.*
453 *Phys.*, 14, 9451-9467, 10.5194/acp-14-9451-2014, 2014.

454 Krueger, B. J., Grassian, V. H., Cowin, J. P., and Laskin, A.: Heterogeneous chemistry of individual mineral dust
455 particles from different dust source regions: the importance of particle mineralogy, *Atmos. Environ.*, 38,
456 6253-6261, 10.1016/j.atmosenv.2004.07.010, 2004.

457 Laskin, A., Iedema, M. J., Ichkovich, A., Graber, E. R., Taraniuk, I., and Rudich, Y.: Direct observation of
458 completely processed calcium carbonate dust particles, *Faraday Discuss.*, 130, 453-468, 10.1039/b417366j, 2005.

459 Lee, Y.-N., and Schwartz, S. E.: Kinetics of oxidation of aqueous sulfur (IV) by nitrogen dioxide, in:
460 *Precipitation Scavenging, Dry Deposition and Resuspension*, edited by: Pruppacher, H. R., Semonin, R. G., and
461 Slinn, W. G. N., Elsevier, New York, 453-466, 1983.

462 Lelieveld, J., Gromov, S., Pozzer, A., and Taraborrelli, D.: Global tropospheric hydroxyl distribution, budget and
463 reactivity, *Atmos. Chem. Phys.*, 16, 12477-12493, 10.5194/acp-16-12477-2016, 2016.

464 Li, H. J., Zhu, T., Zhao, D. F., Zhang, Z. F., and Chen, Z. M.: Kinetics and mechanisms of heterogeneous
465 reaction of NO₂ on CaCO₃ surfaces under dry and wet conditions, *Atmos. Chem. Phys.*, 10, 463-474, 2010.

466 Li, J., Shang, J., and Zhu, T.: Heterogeneous reactions of SO₂ on ZnO particle surfaces, *Sci. China Chem.*, 54,
467 161-166, 10.1007/s11426-010-4167-9, 2011.

468 Li, L., Chen, Z. M., Ding, J., Zhu, T., and Zhang, Y. H.: A DRIFTS study of SO₂ oxidation on the surface of
469 CaCO₃ particles, *Spectrosc. Spect. Anal.*, 24, 1556-1559, 2004.

470 Li, L., Chen, Z. M., Zhang, Y. H., Zhu, T., Li, J. L., and Ding, J.: Kinetics and mechanism of heterogeneous
471 oxidation of sulfur dioxide by ozone on surface of calcium carbonate, *Atmos. Chem. Phys.*, 6, 2453-2464, 2006.

472 Li, L., Chen, Z. M., Zhang, Y. H., Zhu, T., Li, S., Li, H. J., Zhu, L. H., and Xu, B. Y.: Heterogeneous oxidation
473 of sulfur dioxide by ozone on the surface of sodium chloride and its mixtures with other components, *J. Geophys.*
474 *Res.-Atmos.*, 112, 10.1029/2006jd008207, 2007.

475 Li, W. J., and Shao, L. Y.: Observation of nitrate coatings on atmospheric mineral dust particles, *Atmos. Chem.*
476 *Phys.*, 9, 1863-1871, 2009.

477 Lide, D. R.: *CRC Handbook of Chemistry and Physics*, 89 ed., CRC Press/Taylor and Francis, Boca Raton, FL,
478 2009.

479 Littlejohn, D., Wang, Y. Z., and Chang, S. G.: Oxidation of aqueous sulfite ion by nitrogen-dioxide, *Environ. Sci.*
480 *Technol.*, 27, 2162-2167, 10.1021/es00047a024, 1993.

481 Liu, C., Ma, Q. X., Liu, Y. C., Ma, J. Z., and He, H.: Synergistic reaction between SO₂ and NO₂ on mineral
482 oxides: a potential formation pathway of sulfate aerosol, *Phys. Chem. Chem. Phys.*, 14, 1668-1676,
483 10.1039/c1cp22217a, 2012.

484 Liu, M. X., Song, Y., Zhou, T., Xu, Z. Y., Yan, C. Q., Zheng, M., Wu, Z. J., Hu, M., Wu, Y. S., and Zhu, T.: Fine
485 particle pH during severe haze episodes in northern China, *Geophys. Res. Lett.*, 44, 5213-5221,
486 10.1002/2017gl073210, 2017.

487 Liu, Y. J., Zhu, T., Zhao, D. F., and Zhang, Z. F.: Investigation of the hygroscopic properties of Ca(NO₃)(2) and
488 internally mixed Ca(NO₃)(2)/CaCO₃ particles by micro-Raman spectrometry, *Atmos. Chem. Phys.*, 8,
489 7205-7215, 2008.

490 Ma, Q., He, H., Liu, Y., Liu, C., and Grassian, V. H.: Heterogeneous and multiphase formation pathways of
491 gypsum in the atmosphere, *Phys. Chem. Chem. Phys.*, 15, 19196-19204, 10.1039/c3cp53424c, 2013a.

492 Ma, Q., Wang, T., Liu, C., He, H., Wang, Z., Wang, W., and Liang, Y.: SO₂ Initiates the Efficient Conversion of
493 NO₂ to HONO on MgO Surface, *Environ. Sci. Technol.*, 51, 3767-3775, 10.1021/acs.est.6b05724, 2017.

494 Ma, Q. X., Liu, Y. C., and He, H.: Synergistic effect between NO₂ and SO₂ in their adsorption and reaction on
495 gamma-alumina, *J. Phys. Chem. A* 112, 6630-6635, 10.1021/jp802025z, 2008.

496 Ma, Q. X., He, H., Liu, Y. C., Liu, C., and Grassian, V. H.: Heterogeneous and multiphase formation pathways of
497 gypsum in the atmosphere, *Phys. Chem. Chem. Phys.*, 15, 19196-19204, 10.1039/c3cp53424c, 2013b.

498 Martin, L. R., Damschen, D. E., and Judeikis, H. S.: The reactions of nitrogen-oxides with SO₂ in aqueous
499 aerosols, *Atmos. Environ.*, 15, 191-195, 10.1016/0004-6981(81)90010-x, 1981.

500 Meyer, B., Ospina, M., and Peter, L. B.: Raman spectrometric determination of oxysulfur anions in aqueous
501 systems, *Anal. Chim. Acta* 117, 301-311, 10.1016/0003-2670(80)87030-9, 1980.

502 Nakamoto, K.: *Infrared and Raman Spectra of Inorganic and Coordination Compounds*, John Wiley & Sons, New
503 York, 1997.

504 Nash, T.: Effect of nitrogen-dioxide and of some transition-metals on the oxidation of dilute bisulfite solutions,
505 *Atmos. Environ.*, 13, 1149-1154, 10.1016/0004-6981(79)90038-6, 1979.

506 Okada, K., Qin, Y., and Kai, K.: Elemental composition and mixing properties of atmospheric mineral particles
507 collected in Hohhot, China, *Atmos. Res.*, 73, 45-67, 2005.

508 Park, J. Y., and Jang, M.: Heterogeneous photooxidation of sulfur dioxide in the presence of airborne mineral
509 dust particles, *Rsc Advances*, 6, 58617-58627, 10.1039/c6ra09601h, 2016.

510 Passananti, M., Kong, L. D., Shang, J., Dupart, Y., Perrier, S., Chen, J. M., Donaldson, D. J., and George, C.:
511 Organosulfate Formation through the Heterogeneous Reaction of Sulfur Dioxide with Unsaturated Fatty Acids
512 and Long-Chain Alkenes, *Angew. Chem.-Int. Edit.*, 55, 10336-10339, 10.1002/anie.201605266, 2016.

513 Prince, A. P., Grassian, V. H., Kleiber, P., and Young, M. A.: Heterogeneous conversion of calcite aerosol by
514 nitric acid, *Phys. Chem. Chem. Phys.*, 9, 622-634, 2007a.

515 Prince, A. P., Kleiber, P., Grassian, V. H., and Young, M. A.: Heterogeneous interactions of calcite aerosol with
516 sulfur dioxide and sulfur dioxide-nitric acid mixtures, *Phys. Chem. Chem. Phys.*, 9, 3432-3439, 2007b.

517 Prinn, R. G., Huang, J., Weiss, R. F., Cunnold, D. M., Fraser, P. J., Simmonds, P. G., McCulloch, A., Harth, C.,
518 Reimann, S., Salameh, P., O'Doherty, S., Wang, R. H. J., Porter, L. W., Miller, B. R., and Krummel, P. B.:
519 Evidence for variability of atmospheric hydroxyl radicals over the past quarter century, *Geophys. Res. Lett.*, 32,
520 10.1029/2004gl022228, 2005.

521 Rosenberg, H. S., and Grotta, H. M.: Nitrogen oxides (NO_x) influence on sulfite oxidation and scaling in
522 lime/limestone flue gas desulfurization (FGD) systems, *Environ. Sci. Technol.*, 14, 470-472,
523 10.1021/es60164a011, 1980.

524 Sarma, L. P., Prasad, P. S. R., and Ravikumar, N.: Raman spectroscopic study of phase transitions in natural
525 gypsum, *J. Raman Spectrosc.*, 29, 851-856, 10.1002/(sici)1097-4555(199809)29:9<851::aid-jrs313>3.0.co;2-s,
526 1998.

527 Seinfeld, J. H., and Pandis, S. N.: *Atmospheric chemistry and physics: from air pollution to climate change*, 2nd
528 ed., John Wiley & Sons. Inc., 2006.

529 Shang, J., Li, J., and Zhu, T.: Heterogeneous reaction of SO₂ on TiO₂ particles, *Sci. China Chem.*, 53, 2637-2643,
530 10.1007/s11426-010-4160-3, 2010.

531 Shen, C. H., and Rochelle, G. T.: Nitrogen Dioxide Absorption and Sulfite Oxidation in Aqueous Sulfite, *Environ.*
532 *Sci. Technol.*, 32, 1994-2003, 10.1021/es970466q, 1998.

533 Song, C. H., Maxwell-Meier, K., Weber, R. J., Kapustin, V., and Clarke, A.: Dust composition and mixing state
534 inferred from airborne composition measurements during ACE-Asia C130 Flight #6, *Atmos. Environ.*, 39,
535 359-369, 2005.

536 Sorimachi, A., Sakai, M., Ishitani, O., Nishikawa, M., and Sakamoto, K.: Study on dry deposition of SO₂-NO_x
537 onto loess, *Water Air Soil Pollut.*, 130, 541-546, 10.1023/a:1013834729728, 2001.

538 Stafford, R. G., Chang, R. K., and Kindlmann, P. J.: Laser-Raman monitoring of ambient sulfate aerosols, in:
539 *Methods and standards for environmental measurement: Proceedings of the 8th Materials Research Symposium*,
540 edited by: Kirchoff, W. H., National Bureau of Standards, Washington, 1976.

541 Sullivan, R. C., Guazzotti, S. A., Sodeman, D. A., and Prather, K. A.: Direct observations of the atmospheric
542 processing of Asian mineral dust, *Atmos. Chem. Phys.*, 7, 1213-1236, 2007.

543 Takeuchi, H., Ando, M., and Kizawa, N.: Absorption of Nitrogen Oxides in Aqueous Sodium Sulfite and
544 Bisulfite Solutions, *Industrial & Engineering Chemistry Process Design and Development*, 16, 303-308,
545 10.1021/i260063a010, 1977.

546 Tan, F., Jing, B., Tong, S. R., and Ge, M. F.: The effects of coexisting Na₂SO₄ on heterogeneous uptake of NO₂
547 on CaCO₃ particles at various RHs, *Sci. Total Environ.*, 586, 930-938, 10.1016/j.scitotenv.2017.02.072, 2017.

548 Tang, I. N., and Fung, K. H.: Hydration and Raman scattering studies of levitated microparticles: Ba(NO₃)(₂),
549 Sr(NO₃)(₂), and Ca(NO₃)(₂), *J. Chem. Phys.*, 106, 1653-1660, 1997.

550 Tursic, J., and Grgic, I.: Influence of NO₂ on S(IV) oxidation in aqueous suspensions of aerosol particles from
551 two different origins, *Atmos. Environ.*, 35, 3897-3904, 10.1016/s1352-2310(01)00142-x, 2001.

552 Ullerstam, M., Vogt, R., Langer, S., and Ljungstrom, E.: The kinetics and mechanism of SO₂ oxidation by O₃
553 on mineral dust, *Phys. Chem. Chem. Phys.*, 4, 4694-4699, 10.1039/b203529b, 2002.

554 Ullerstam, M., Johnson, M. S., Vogt, R., and Ljungstrom, E.: DRIFTS and Knudsen cell study of the
555 heterogeneous reactivity of SO₂ and NO₂ on mineral dust, *Atmos. Chem. Phys.*, 3, 2043-2051, 2003.

556 Wang, G., Zhang, R., Gomez, M. E., Yang, L., Levy Zamora, M., Hu, M., Lin, Y., Peng, J., Guo, S., Meng, J., Li,
557 J., Cheng, C., Hu, T., Ren, Y., Wang, Y., Gao, J., Cao, J., An, Z., Zhou, W., Li, G., Wang, J., Tian, P.,
558 Marrero-Ortiz, W., Secrest, J., Du, Z., Zheng, J., Shang, D., Zeng, L., Shao, M., Wang, W., Huang, Y., Wang, Y.,
559 Zhu, Y., Li, Y., Hu, J., Pan, B., Cai, L., Cheng, Y., Ji, Y., Zhang, F., Rosenfeld, D., Liss, P. S., Duce, R. A., Kolb,
560 C. E., and Molina, M. J.: Persistent sulfate formation from London Fog to Chinese haze, *Proc. Nat. Acad. Sci.*
561 *U.S.A.*, 113, 13630-13635, 10.1073/pnas.1616540113, 2016.

562 Wang, Y. S., Yao, L., Wang, L. L., Liu, Z. R., Ji, D. S., Tang, G. Q., Zhang, J. K., Sun, Y., Hu, B., and Xin, J. Y.:
563 Mechanism for the formation of the January 2013 heavy haze pollution episode over central and eastern China,
564 *Sci. China Earth Sci.*, 57, 14-25, 10.1007/s11430-013-4773-4, 2014a.

565 Wang, Y. X., Zhang, Q. Q., Jiang, J. K., Zhou, W., Wang, B. Y., He, K. B., Duan, F. K., Zhang, Q., Philip, S.,
566 and Xie, Y. Y.: Enhanced sulfate formation during China's severe winter haze episode in January 2013 missing
567 from current models, *J. Geophys. Res.-Atmos.*, 119, 10.1002/2013jd021426, 2014b.

568 Weber, R. J., Guo, H. Y., Russell, A. G., and Nenes, A.: High aerosol acidity despite declining atmospheric
569 sulfate concentrations over the past 15 years, *Nat. Geosci.*, 9, 282+, 10.1038/ngeo2665, 2016.

570 Wehner, B., Birmili, W., Ditas, F., Wu, Z., Hu, M., Liu, X., Mao, J., Sugimoto, N., and Wiedensohler, A.:
571 Relationships between submicrometer particulate air pollution and air mass history in Beijing, China, 2004 -
572 2006, *Atmos. Chem. Phys.*, 8, 6155-6168, 10.5194/acp-8-6155-2008, 2008.

573 Wright, M. L.: Feasibility study of in-situ source monitoring of particulate composition by Raman or fluorescence
574 scatter, Washington, D.C., 1973.

575 Wu, L. Y., Tong, S. R., Wang, W. G., and Ge, M. F.: Effects of temperature on the heterogeneous oxidation of
576 sulfur dioxide by ozone on calcium carbonate, *Atmos. Chem. Phys.*, 11, 6593-6605, 10.5194/acp-11-6593-2011,
577 2011.

578 Wu, L. Y., Tong, S. R., Zhou, L., Wang, W. G., and Ge, M. F.: Synergistic Effects between SO₂ and HCOOH on
579 alpha-Fe₂O₃, *J. Phys. Chem. A* 117, 3972-3979, 10.1021/jp400195f, 2013.

580 Wu, L. Y., Tong, S. R., and Ge, M. F.: Synergistic Effect between SO₂ and HCOOH on the Surface of CaO, *Acta*
581 *Chim. Sinica* 73, 131-136, 10.6023/a14120875, 2015.

582 Xie, Y. N., Ding, A. J., Nie, W., Mao, H. T., Qi, X. M., Huang, X., Xu, Z., Kerminen, V. M., Petaja, T., Chi, X.
583 G., Virkkula, A., Boy, M., Xue, L. K., Guo, J., Sun, J. N., Yang, X. Q., Kulmala, M., and Fu, C. B.: Enhanced
584 sulfate formation by nitrogen dioxide: Implications from in situ observations at the SORPES station, *J. Geophys.*
585 *Res.-Atmos.*, 120, 12679-12694, 10.1002/2015jd023607, 2015.

586 Xue, J., Yuan, Z. B., Griffith, S. M., Yu, X., Lau, A. K. H., and Yu, J. Z.: Sulfate Formation Enhanced by a
587 Cocktail of High NO_x, SO₂, Particulate Matter, and Droplet pH during Haze-Fog Events in Megacities in China:
588 An Observation-Based Modeling Investigation, *Environ. Sci. Technol.*, 50, 7325-7334, 10.1021/acs.est.6b00768,
589 2016.

590 Young, A. H., Keene, W. C., Pszenny, A. A. P., Sander, R., Thornton, J. A., Riedel, T. P., and Maben, J. R.:
591 Phase partitioning of soluble trace gases with size-resolved aerosols in near-surface continental air over northern
592 Colorado, USA, during winter, *J. Geophys. Res.-Atmos.*, 118, 9414-9427, 10.1002/jgrd.50655, 2013.

593 Zhang, D. Z., Shi, G. Y., Iwasaka, Y., and Hu, M.: Mixture of sulfate and nitrate in coastal atmospheric aerosols:
594 individual particle studies in Qingdao (36 degrees 04 ' N, 120 degrees 21 ' E), China, *Atmos. Environ.*, 34,
595 2669-2679, 10.1016/s1352-2310(00)00078-9, 2000.

596 Zhang, D. Z., Zang, J. Y., Shi, G. Y., Iwasaka, Y., Matsuki, A., and Trochkin, D.: Mixture state of individual
597 Asian dust particles at a coastal site of Qingdao, China, *Atmos. Environ.*, 37, 3895-3901,
598 10.1016/s1352-2310(03)00506-5, 2003.

599 Zhang, J. K., Sun, Y., Liu, Z. R., Ji, D. S., Hu, B., Liu, Q., and Wang, Y. S.: Characterization of submicron
600 aerosols during a month of serious pollution in Beijing, 2013, *Atmos. Chem. Phys.*, 14, 2887-2903,
601 10.5194/acp-14-2887-2014, 2014.

602 Zhang, Q., Jimenez, J. L., Canagaratna, M. R., Allan, J. D., Coe, H., Ulbrich, I., Alfarra, M. R., Takami, A.,
603 Middlebrook, A. M., Sun, Y. L., Dzepina, K., Dunlea, E., Docherty, K., DeCarlo, P. F., Salcedo, D., Onasch, T.,
604 Jayne, J. T., Miyoshi, T., Shimojo, A., Hatakeyama, S., Takegawa, N., Kondo, Y., Schneider, J., Drewnick, F.,
605 Borrmann, S., Weimer, S., Demerjian, K., Williams, P., Bower, K., Bahreini, R., Cottrell, L., Griffin, R. J.,
606 Rautiainen, J., Sun, J. Y., Zhang, Y. M., and Worsnop, D. R.: Ubiquity and dominance of oxygenated species in
607 organic aerosols in anthropogenically-influenced Northern Hemisphere midlatitudes, *Geophys. Res. Lett.*, 34,
608 10.1029/2007gl029979, 2007.

609 Zhao, D. F., Zhu, T., Chen, Q., Liu, Y. J., and Zhang, Z. F.: Raman micro-spectrometry as a technique for
610 investigating heterogeneous reactions on individual atmospheric particles, *Sci. China Chem.*, 54, 154-160,
611 10.1007/s11426-010-4182-x, 2011.

612 Zhao, X., Kong, L. D., Sun, Z. Y., Ding, X. X., Cheng, T. T., Yang, X., and Chen, J. M.: Interactions between
613 Heterogeneous Uptake and Adsorption of Sulfur Dioxide and Acetaldehyde on Hematite, *J. Phys. Chem. A* 119,
614 4001-4008, 10.1021/acs.jpca.5b01359, 2015.

615 Zheng, B., Zhang, Q., Zhang, Y., He, K. B., Wang, K., Zheng, G. J., Duan, F. K., Ma, Y. L., and Kimoto, T.:
616 Heterogeneous chemistry: a mechanism missing in current models to explain secondary inorganic aerosol
617 formation during the January 2013 haze episode in North China, *Atmos. Chem. Phys.*, 15, 2031-2049,
618 10.5194/acp-15-2031-2015, 2015a.

619 Zheng, G. J., Duan, F. K., Su, H., Ma, Y. L., Cheng, Y., Zheng, B., Zhang, Q., Huang, T., Kimoto, T., Chang, D.,
620 Poschl, U., Cheng, Y. F., and He, K. B.: Exploring the severe winter haze in Beijing: the impact of synoptic

621 weather, regional transport and heterogeneous reactions, *Atmos. Chem. Phys.*, 15, 2969-2983,
622 10.5194/acp-15-2969-2015, 2015b.

623 Zhou, L., Wang, W. G., Gai, Y. B., and Ge, M. F.: Knudsen cell and smog chamber study of the heterogeneous
624 uptake of sulfur dioxide on Chinese mineral dust, *J. Environ. Sci.*, 26, 2423-2433, 10.1016/j.jes.2014.04.005,
625 2014.

626 Zhu, T., Shang, J., and Zhao, D. F.: The roles of heterogeneous chemical processes in the formation of an air
627 pollution complex and gray haze, *Sci. China Chem.*, 54, 145-153, 10.1007/s11426-010-4181-y, 2011.

628

629

Table 1 Summary of the results obtained in different reaction systems

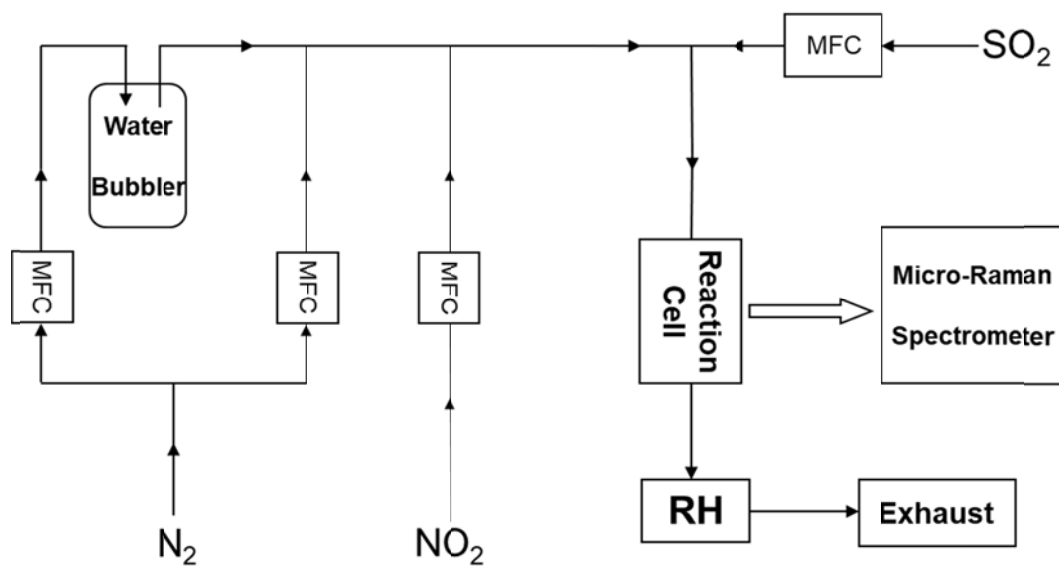
Particle	Gases	RH (%)	Whether sulfate was detected
CaCO ₃	SO ₂ (75 ppm)+NO ₂ (75 ppm)	72	Yes
Ca(NO ₃) ₂ droplet	SO ₂ (75 ppm)+NO ₂ (75 ppm)	72	Yes
CaCO ₃	SO ₂ (150 ppm)	72	No
Ca(NO ₃) ₂ droplet	SO ₂ (150 ppm))	72	No
NaNO ₃ droplet	SO ₂ (75 ppm)+NO ₂ (75 ppm)	72	No
NH ₄ NO ₃ droplet	SO ₂ (75 ppm)+NO ₂ (75 ppm)	72	No

633 Table 2. Reactive uptake coefficient of SO₂ for sulfate formation (γ) during the reaction of SO₂ with NO₂ on
634 individual CaCO₃ particles under different conditions at 298 K.

[SO ₂] (ppm)	[NO ₂] (ppm)	RH (%)	$\gamma (\times 10^{-8})$
75	75	72	3.22±1.08 ^b
75	200	72	16.0±3.12
75	75	46	3.22±0.90
75	75	17	0 ^a
200	200	17	0 ^a

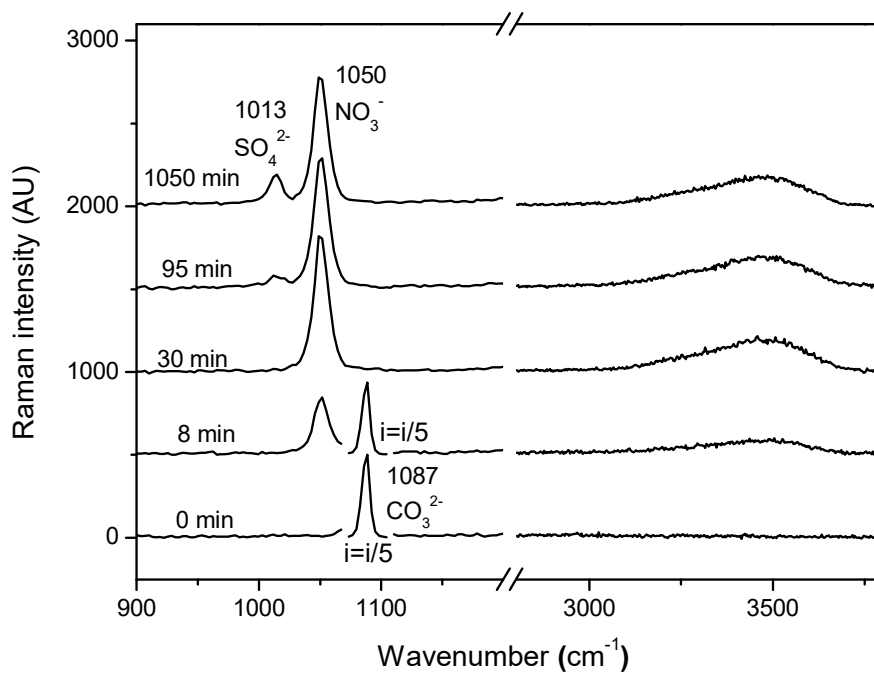
635 ^a: Sulfate was below the detection limit.

636 ^b: The uncertainties are the standard deviations of γ from duplicate experiments.



637

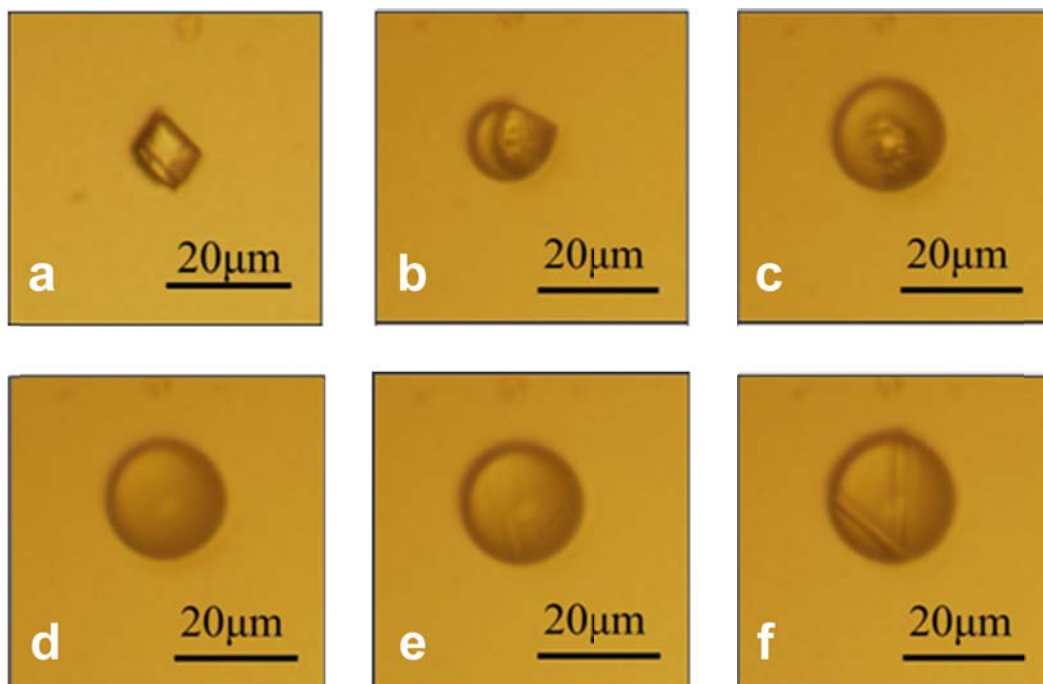
638 Fig. 1. Schematic diagram of the experimental setup. MFC: mass flow controller.



639

640 Fig. 2. Raman spectra of an individual CaCO_3 particle during the reaction with NO_2 (75 ppm) and SO_2 (75 ppm)

641 at 72% RH at the reaction time of 0, 8, 30, 95, and 1050 min.



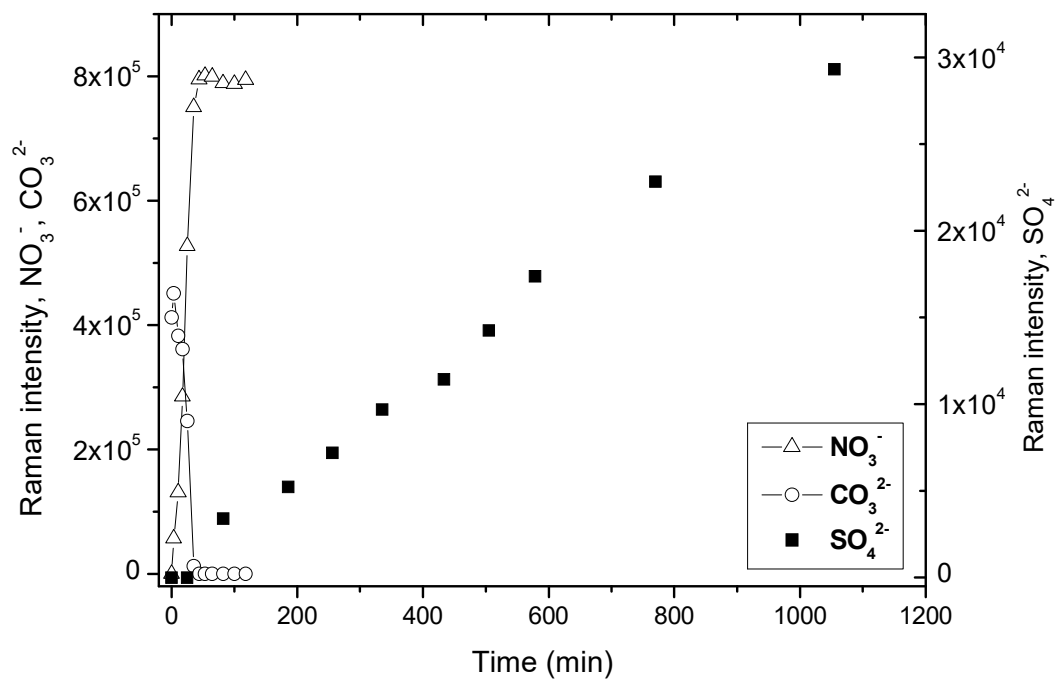
642

643

644

645

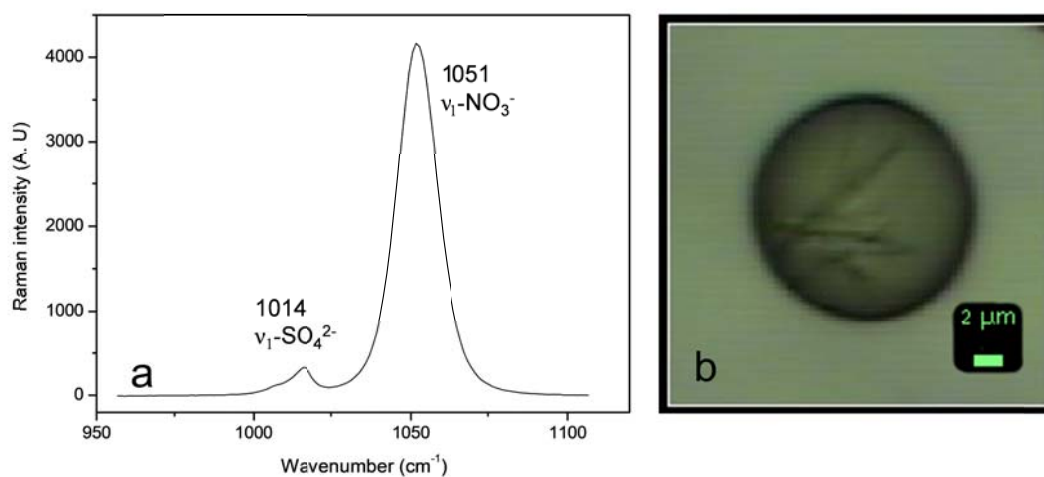
Fig. 3. Microscopic images of an individual CaCO_3 particle (same as in Fig. 2) reacting with NO_2 (75 ppm) and SO_2 (75 ppm) at 72% RH. a-f corresponds to the reaction time of 0, 6, 29, 37, 94, and 1050 min, respectively.



646

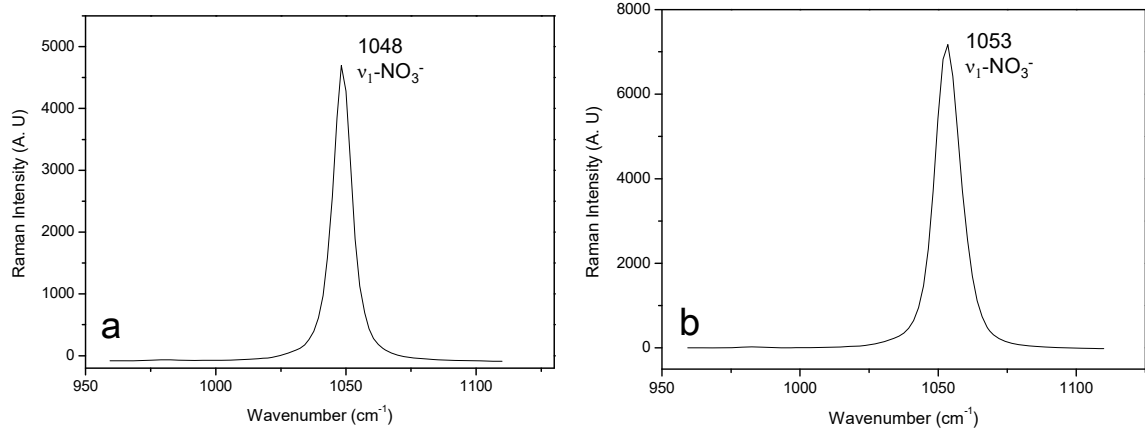
647 Fig. 4. Raman peak intensity of carbonate, nitrate (left axis), and sulfate (right axis) as a function of time during
 648 the reaction of an individual CaCO₃ particle with NO₂ (75ppm) and SO₂ (75ppm) at 72% RH (same as in Fig. 2
 649 and 3). Note that the scales of the left axis and right axis are different. The intensity of NO₃⁻, SO₄²⁻, and CO₃²⁻
 650 show the peak area at 1050, 1013, and 1087 cm⁻¹, respectively, in Raman spectra obtained by Raman mapping.
 651 By 118 min, CaCO₃ was completely converted to Ca(NO₃)₂. Carbonate had decreased to zero and nitrate had
 652 reached a plateau. Therefore no further data of carbonate and nitrate were shown.

653



655

656 Fig. 5. Raman spectra (a) and microscopic image (b) of a $\text{Ca}(\text{NO}_3)_2$ droplet reacting with NO_2 (75 ppm) and SO_2
657 (75 ppm) at 72% RH at a reaction time of 300 min. The peak at 1014 cm^{-1} in Raman spectra and crystals from the
658 microscopic image indicate CaSO_4 was formed in this reaction.



660

661 Fig. 6. Raman spectra of a NH_4NO_3 (a) and NaNO_3 (b) droplet reacting with NO_2 (75 ppm) and SO_2 (75 ppm) at
662 72% RH at the reaction time of 300 min.

663